Structure Preserving Reduction of Frequency-dependent Interconnect

Quming Zhou
quming@rice.edu

Kartik Mohanram
kmram@rice.edu

Athanasios C. Antoulas
aca@rice.edu

Department of Electrical and Computer Engineering
Rice University, Houston, TX 77005

ABSTRACT

A rational Arnoldi method for passivity-preserving model-order reduction (MOR) with implicit multi-point moment matching for systems with frequency-dependent interconnects is described. The structure $\mathbf{H}(s) = s\mathbf{E} - \mathbf{A} - \mathbf{K}\sqrt{f}$, which arises from frequency-dependent effects in high speed interconnects, is preserved by the proposed MOR technique. Moment matching using congruence transforms and based on two types of moments that are derivatives of the transfer function w.r.t s and $\sqrt{f}$ is described. Simulation results show that the proposed approach can significantly reduce the complexity of systems with frequency-dependent elements, while retaining high accuracy in comparison to the original system in both the time and frequency domains.

Categories and Subject Descriptors: B.7.2 [Integrated circuits]: Design aids—simulation
General Terms: Algorithms
Keywords: Model-order reduction, skin effect, interconnect

1. INTRODUCTION

Model-order reduction (MOR) techniques have been used extensively in integrated circuit design to reduce the complexity of extracted interconnect circuits and to expedite simulation. Examples of such techniques include first-order MOR techniques like AWE [1] based on explicit moment matching and more recently, PRIMA [2], PVL [3], and their derivatives that use Arnoldi and Lanczos processes to compute Krylov space and Padé based approximations of the original system. Recently, MOR techniques based on spectral zeroes [4] and MOR techniques for second-order systems have also been proposed [5, 6, 7]. All these techniques focus on the reduction of systems with constant RLC elements. However, circuits with frequency-dependent elements (e.g., circuits modeling the skin effect) cannot be solved by current techniques because frequency-dependent effects couple the time and frequency domains. Consequently, the matrices describing the system have a $\sqrt{f}$ structure that cannot be transformed into conventional first-order or second-order structures.

DAC 2005, June 13–17, 2005, Anaheim, California, USA.

In [8], the concept of square root moments was introduced to handle frequency-dependent impedances due to the skin effect. The main disadvantage of this technique is that stability and passivity cannot be preserved by the Padé via Lanczos (PVL) procedure used in the paper. The other significant drawback is that the reference point chosen for expansion ($s = 0$) is not appropriate for modeling the skin effect in interconnects, since it is significant only at high frequencies of operation.

The main contribution of this paper is a rational Arnoldi method for passivity-preserving MOR with implicit multi-point moment matching for systems with frequency-dependent interconnects. We address interconnects with skin effect in the paper; however, the proposed algorithm can be equally applied to MOR of other classes of interconnect and microwave circuits. The structure $\mathbf{H}(s) = s\mathbf{E} - \mathbf{A} - \mathbf{K}\sqrt{f}$, which arises from the skin effect in high speed interconnects, is preserved by the proposed MOR technique. Moment matching using congruence transforms and based on two types of moments that are derivatives of the transfer function w.r.t s and $\sqrt{f}$ is described. The reduced system preserves the frequency-dependent structure of the original system in addition to stability and passivity. The reason for the use of multi-point expansion to model the frequency-dependent nature of resistance is that such an expansion will generate a more accurate approximation over a wide range of frequencies than that through a single-point expansion. Simulation results with FFT/IFFT computations show that the proposed approach can significantly reduce the complexity of systems with frequency-dependent elements, while retaining high accuracy in comparison to the original system in both the time and frequency domains.

2. BACKGROUND

The exact model for skin effect is very complex to be included in the KCL and KVL equations used to solve large circuits. Conventionally, frequency dependence of interconnect resistance has been expressed by the square root function. A single parameter $\sqrt{f}$-based approximation

$$R(f) = R_0 + k\sqrt{f} \tag{1}$$

for the resistance is shown by the dotted curve in Fig. 1. However, this is not an accurate approximation over a large range of operating frequencies. In this paper, we use a piece-wise approximation for frequency-dependent resistance over the range of frequencies of interest (shown using the dash-dot curve in Fig. 1). The frequency range is divided into four regions 0–0.1 GHz, 0.1–1 GHz, 1–10 GHz, and 10–100 GHz. Over each frequency range, we approximate the resistance using Eqn. 1 to achieve high accuracy. Those frequency boundaries 0, 0.1 GHz, 1 GHz and 10 GHz, are

the candidates for multi-point expansion of the transfer function during the MOR phase. Note that inductance decreases marginally over this range of frequencies and is assumed to be independent of frequency in this analysis.

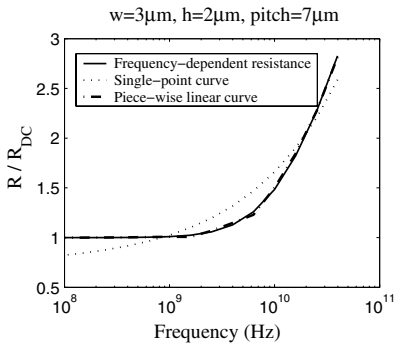

Figure 1: Normalized frequency-dependent resistance.

Consider a p-port distributed RLC circuit that models interconnects with frequency-dependent resistance due to the skin effect. The circuit is driven by p voltage sources. Circuit analysis techniques focus on the computation of the driving point admittance matrix of this system. The state space model for the RLC circuit with frequency-dependent resistance elements is given by

$$\mathbf{E}\dot{\mathbf{x}}(t) = \left(\mathbf{A} + \mathbf{K}\sqrt{f}\right)\mathbf{x}(t) + \mathbf{B}\mathbf{u}(t) \text{ and } \mathbf{y}(t) = \mathbf{B}^{\mathrm{T}}\mathbf{x}(t) \quad (2)$$

where $\mathbf{x}(t) \in \Re^n$ is the state, $\mathbf{u}(t) \in \Re^p$ is the input, and $\mathbf{y}(t) \in \Re^p$ is the output of the system at time t. $\mathbf{A}$, $\mathbf{B}$, and $\mathbf{E}$ are constant matrices. $\mathbf{K}$ is the frequency coefficient matrix of resistance and f is the frequency of operation. The transfer function of the original system defined by Eqn. 2 is

$$\mathbf{G}(s) = \mathbf{B}^{\mathrm{T}}\left(s\mathbf{E} - \mathbf{A} - \mathbf{K}\sqrt{f}\right)^{-1}\mathbf{B} \quad (3)$$

and the frequency-dependent structure for the original system is defined as

$$\mathbf{H}(s) = s\mathbf{E} - \mathbf{A} - \mathbf{K}\sqrt{f} \quad (4)$$

Structure-preserving MOR seeks corresponding $\hat{\mathbf{A}}$, $\hat{\mathbf{B}}$, $\hat{\mathbf{E}}$, and $\hat{\mathbf{K}}$ to represent the reduced system that satisfies the following:

$$\hat{\mathbf{E}}\dot{\hat{\mathbf{x}}}(t) = \left(\hat{\mathbf{A}} + \hat{\mathbf{K}}\sqrt{f}\right)\hat{\mathbf{x}}(t) + \hat{\mathbf{B}}\mathbf{u}(t) \text{ and } \hat{\mathbf{y}}(t) = \mathbf{B}^{\mathrm{T}}\hat{\mathbf{x}}(t) \quad (5)$$

where $\hat{\mathbf{x}}(t) \in \Re^{n_r}$ with a complexity $n_r \ll n$. The frequency-dependent structure for the reduced systems is defined as

$$\hat{\mathbf{H}}(s) = s\hat{\mathbf{E}} - \hat{\mathbf{A}} - \hat{\mathbf{K}}\sqrt{f}. \quad (6)$$

The reduced system retains the original structure with frequency-dependent resistance, but with much smaller complexity. Based on the reduced system, fast Fourier transform (FFT) or full-wave analysis [9] can be implemented to obtain the response in the time domain at a computational cost that is far less in comparison to that of the original system.

3. RATIONAL KRYLOV INTERPOLATION

In this section, structure-preserving MOR using a congruence transform and multi-point interpolation is described. The Krylov-based projection method interpolates the transfer function at multiple interpolation points and their $q-1$ derivatives, where q is a given number. By expanding at multiple frequency points, the original system is accurately approximated in both the frequency and time domains [10].

We construct an orthonormal $n \times n_r$ dimensional projection matrix $\mathbf{V}$ and define the congruence transform as

$$\hat{\mathbf{A}} = \mathbf{V}^{\mathrm{T}}\mathbf{A}\mathbf{V}, \hat{\mathbf{B}} = \mathbf{V}^{\mathrm{T}}\mathbf{B}, \hat{\mathbf{E}} = \mathbf{V}^{\mathrm{T}}\mathbf{E}\mathbf{V}, \hat{\mathbf{K}} = \mathbf{V}^{\mathrm{T}}\mathbf{K}\mathbf{V}. \quad (7)$$

The reduced transfer function is then given by

$$\hat{\mathbf{G}}(s) = \hat{\mathbf{B}}^{\mathrm{T}}(s\hat{\mathbf{E}} - \hat{\mathbf{A}} - \hat{\mathbf{K}}\sqrt{f})^{-1}\hat{\mathbf{B}}. \quad (8)$$

THEOREM 3.1. *The projection operator defined in Eqn. 7 is passivity preserving, i.e., the reduced transfer function given by $\hat{\mathbf{G}}(s)$ is passive given that the original system represented by the transfer function $\mathbf{G}(s)$ is passive.*

PROOF. The proof is omitted here for brevity. □

3.1 Krylov Space

We are interested in a reduced system that interpolates the frequency response and its moments at multiple interpolation points $\{\sigma_1, \sigma_2, \cdots, \sigma_r\}$. Note that each σ corresponds to a complex frequency jw. For each σ, in order to obtain real matrices $\hat{\mathbf{A}}$, $\hat{\mathbf{B}}$, $\hat{\mathbf{E}}$, and $\hat{\mathbf{K}}$, we also need to interpolate at the complex conjugate frequency $-\sigma$. $\mathbf{H}(s)$ is assumed non-singular at $\pm\sigma$. Since we have two variables s and $\sqrt{f}$, we define two types of moments based on s and $\sqrt{f}$ respectively for each interpolation point σ.

Type I moments $\mathbf{m}_j^{\mathrm{I}}$ are defined as the coefficients of s in the power series expansion for $\mathbf{G}(s)$ about σ given by

$$\mathbf{G}(s) = \mathbf{B}^{\mathrm{T}}\mathbf{H}^{-1}\mathbf{B} = \sum\nolimits_{j=0}^{\infty}(s-\sigma)^j\mathbf{m}_j^{\mathrm{I}}$$
$$\text{where } \mathbf{m}_j^{\mathrm{I}} = (-1)^j\mathbf{B}^{\mathrm{T}}\{\mathbf{H}^{-1}(\sigma)\mathbf{E}\}^j\mathbf{H}^{-1}(\sigma)\mathbf{B}.$$

In a similar manner, type II moments $\mathbf{m}_j^{\mathrm{II}}$ are given by the coefficients of $\sqrt{f}$ in the power series expansion for $\mathbf{G}(s)$ about σ as

$$\mathbf{G}(s) = \mathbf{B}^{\mathrm{T}}\mathbf{H}^{-1}\mathbf{B} = \sum\nolimits_{j=0}^{\infty}\left(\sqrt{f} - \sqrt{\mathrm{Im}(\sigma)}\right)^j\mathbf{m}_j^{\mathrm{II}}$$
$$\text{where } \mathbf{m}_j^{\mathrm{II}} = \mathbf{B}^{\mathrm{T}}\{\mathbf{H}^{-1}(\sigma)\mathbf{K}\}^j\mathbf{H}^{-1}(\sigma)\mathbf{B}.$$

The reduced transfer function $\hat{\mathbf{G}}(s)$ is required to have the same moments up to a given order q at each interpolation point σ. In order to maintain the structure w.r.t $\sqrt{f}$ in the reduced system, the matching conditions are given in terms of type I and type II moments respectively, as

$$\mathbf{m}_j^{\mathrm{I}} = \hat{\mathbf{m}}_j^{\mathrm{I}} \text{ and } \mathbf{m}_j^{\mathrm{II}} = \hat{\mathbf{m}}_j^{\mathrm{II}} \text{ for } 0 \le j < q, \quad (9)$$

where the reduced moments $\hat{\mathbf{m}}_j^{\mathrm{I}}$ and $\hat{\mathbf{m}}_j^{\mathrm{II}}$ are defined in terms of $[\hat{\mathbf{A}}, \hat{\mathbf{B}}, \hat{\mathbf{E}}, \hat{\mathbf{K}}]$ and q is the number of moments that are sought at σ.

For each point $\sigma \in \{\sigma_1, \sigma_2, \cdots, \sigma_r\}$, we construct a block Krylov subspace $\mathrm{Kr}_{q,\sigma}^{\mathrm{I}}(\mathbf{M}, \mathbf{N})$ spanned by the columns of the matrices

$$\mathrm{Kr}_{q,\sigma}^{\mathrm{I}}(\mathbf{M}, \mathbf{N}) = \mathrm{colspan}\{\mathbf{N}, \mathbf{M}\mathbf{N}, \cdots, \mathbf{M}^{q-1}\mathbf{N}\}, \quad (10)$$

where $\mathbf{M} = \mathbf{H}^{-1}(\sigma)\mathbf{E}$ and $\mathbf{N} = \mathbf{H}^{-1}(\sigma)\mathbf{B}$. Similarly, for each point $\sigma \in \{\sigma_1, \sigma_2, \cdots, \sigma_r\}$, we construct a block Krylov subspace $\mathrm{Kr}_{q,\sigma}^{\mathrm{II}}(\mathbf{M}, \mathbf{N})$ spanned by the columns of the matrices

$$\mathrm{Kr}_{q,\sigma}^{\mathrm{II}}(\mathbf{M}, \mathbf{N}) = \mathrm{colspan}\{\mathbf{N}, \mathbf{M}\mathbf{N}, \cdots, \mathbf{M}^{q-1}\mathbf{N}\}, \quad (11)$$

where $\mathbf{M} = \mathbf{H}^{-1}(\sigma)\mathbf{K}$ and $\mathbf{N} = \mathbf{H}^{-1}(\sigma)\mathbf{B}$. Note that

$$\mathrm{colspan}\left\{\mathrm{Kr}_{q,\sigma}, \mathrm{Kr}_{q,-\sigma}\right\} \equiv \mathrm{colspan}\left\{\mathrm{Re}\left(\mathrm{Kr}_{q,\sigma}\right), \mathrm{Im}\left(\mathrm{Kr}_{q,\sigma}\right)\right\}$$

for both type I and type II moments, and that this implicitly yields moment matching at $-\sigma$. Hence, the block Krylov subspaces constructed using this procedure are real. The major advantage of Krylov methods is that they allow moment matching without explicit computation of moments, whereas direct or recursive calculation of moments is numerically unstable. The column space of the projection matrix $\mathbf{V}$ is composed of multiple Krylov subspaces, which differ by the choice of σ. Matching moments about multiple points requires the use of multiple block Krylov subspaces. The rigorous discussion of moment matching through the union of multiple Krylov subspaces has been described in [11] and [12]. Let $\mathbf{V}$ be a full-rank matrix whose columns belong to

$$\bigcup_{i=1}^{r} \{\mathrm{Kr}^{\mathrm{I}}_{q,\sigma_i}(\mathbf{M},\mathbf{N}), \mathrm{Kr}^{\mathrm{II}}_{q,\sigma_i}(\mathbf{M},\mathbf{N})\}. \tag{12}$$

It follows directly that any $\bar{\mathbf{V}}$ that spans the same column space as $\mathbf{V}$ can be used as a projection matrix. This is formalized by the following propositions:

PROPOSITION 3.2. *If* $\mathrm{range}(\bar{\mathbf{V}}) = \mathrm{range}(\mathbf{V})$*, the two reduced transfer functions defined by Eqn. 8 are equivalent.*

PROOF. The proof is omitted here for brevity. □

PROPOSITION 3.3. *Let* $\mathrm{Kr}^{\mathrm{I}}_{q,\sigma}(\mathbf{M},\mathbf{N}) \subseteq \mathrm{colspan}\{\mathbf{V}\}$*. The reduced system via Eqn. 7 matches the first q type I moments at σ, i.e.,* $\hat{\mathbf{m}}^{\mathrm{I}}_j = \mathbf{m}^{\mathrm{I}}_j$ *for all* $j = 0, 1, \cdots, q-1$.

PROOF. The proof is omitted here for brevity. □

Similar properties are obtained for $\hat{\mathbf{m}}^{\mathrm{II}}_j$ when $\mathrm{Kr}^{\mathrm{II}}_{q,\sigma}(\mathbf{M},\mathbf{N})$ is used to construct $\mathbf{V}$. The above propositions can be interpreted as rational Arnoldi. Its numerical implementation requires combining regular block Arnoldi with shift-invert Arnoldi for the shifts (interpolation points) $\{\sigma_1, \sigma_2, \cdots, \sigma_r\}$. Note that at each σ, only the basis for $\mathrm{Kr}^{\mathrm{I}}_{q,\sigma}(\mathbf{M},\mathbf{N})$ and $\mathrm{Kr}^{\mathrm{II}}_{q,\sigma}(\mathbf{M},\mathbf{N})$ are relevant to type I and type II moments respectively.

3.2 Rational Arnoldi

Constructing a block Krylov subspace for a single interpolation point is implemented by the single-point block rational Arnoldi method SINGLE-POINT-RATIONAL-ARNOLDI (SPRA) presented in Fig. 2. Note that the number of moments q sought at an interpolation point for type I and type II moments may be different.

$[\mathbf{A}, \mathbf{B}, \mathbf{E}, \mathbf{K}]$ – Original system
σ – Interpolation point
$\mathbf{V}$ – Projection matrix

$[\mathbf{L}, \mathbf{U}] \leftarrow$ LU-DECOMPOSE$(\mathbf{H}(\sigma))$
$\mathbf{v} \leftarrow$ NORMALIZE$(\mathbf{U}\backslash(\mathbf{L}\backslash\mathbf{B}))$
$\mathbf{V} \leftarrow$ORTH$([\mathrm{Re}(\mathbf{v}), \mathrm{Im}(\mathbf{v})])$
$\mathbf{v}^{\mathrm{I}} \leftarrow \mathbf{v}$ and $\mathbf{v}^{\mathrm{II}} \leftarrow \mathbf{v}$

for $j \leftarrow 1$ **to** $q-1$
  do $\mathbf{w}^{\mathrm{I}} \leftarrow \mathbf{U}\backslash(\mathbf{L}\backslash(\mathbf{E}\mathbf{v}^{\mathrm{I}}))$
    $\mathbf{v}^{\mathrm{I}} \leftarrow$ NORMALIZE$(\mathbf{w}^{\mathrm{I}} - \mathbf{V}\mathbf{V}^{\mathrm{T}}\mathbf{w}^{\mathrm{I}})$
    $\mathbf{V} \leftarrow [\mathbf{V},$ ORTH$([\mathrm{Re}(\mathbf{v}^{\mathrm{I}}), \mathrm{Im}(\mathbf{v}^{\mathrm{I}})])]$
    $\mathbf{w}^{\mathrm{II}} \leftarrow \mathbf{U}\backslash(\mathbf{L}\backslash(\mathbf{K}\mathbf{v}^{\mathrm{II}}))$
    $\mathbf{v}^{\mathrm{II}} \leftarrow$NORMALIZE$(\mathbf{w}^{\mathrm{II}} - \mathbf{V}\mathbf{V}^{\mathrm{T}}\mathbf{w}^{\mathrm{II}})$
    $\mathbf{V} \leftarrow [\mathbf{V},$ ORTH$([\mathrm{Re}(\mathbf{v}^{\mathrm{II}}), \mathrm{Im}(\mathbf{v}^{\mathrm{II}})])]$

Figure 2: SINGLE-POINT-RATIONAL-ARNOLDI (SPRA)

For multi-point interpolation with $\{\sigma_1, \sigma_2, \cdots, \sigma_r\}$, the Krylov space $\mathbf{V}$ is the union of the individual Krylov subspaces at those points, where the Krylov subspace at each σ is constructed using algorithm SPRA presented in Fig. 2. Rational interpolation is achieved when the column spaces of the final projection matrix $\mathbf{V}$ span the union of the individual Krylov subspaces. In Fig. 3, we present the pseudo-code for the algorithm MULTIPLE-POINT-RATIONAL-ARNOLDI (MPRA) used to construct the union of Krylov subspaces obtained using SPRA.

$[\mathbf{A}, \mathbf{B}, \mathbf{E}, \mathbf{K}]$ – Original system
$\sigma_1, \sigma_2, \ldots, \sigma_r$ – Interpolation points
$\mathbf{V}$ – Projection matrix

$\mathbf{V} \leftarrow$ SPRA$([\mathbf{A}, \mathbf{B}, \mathbf{E}, \mathbf{K}], \sigma_1)$

for $i \leftarrow 2$ **to** r
  do $\mathbf{V} \leftarrow [\mathbf{V},$ SPRA $([\mathbf{A}, \mathbf{B}, \mathbf{E}, \mathbf{K}], \sigma_i)]$
    $\mathbf{V} \leftarrow$ ORTH$(\mathbf{V})$

Figure 3: MULTIPLE-POINT-RATIONAL-ARNOLDI (MPRA)

The operator ORTH refers to orthonormalization, which can be performed by the (modified) Gram-Schmidt algorithm, by QR factorization, or by singular value decomposition. In finite precision, linear dependencies among different Krylov subspaces due to the different interpolation points may happen. The procedure to remove these linear dependencies in $\mathbf{V}$ is called deflation [13]. One of the simplest techniques is to deflate columns whose norm is less than a specified tolerance in QR decomposition. When deflation is performed, the exact moments that are matched at a particular interpolation point may differ from what is expected when the original Krylov subspaces are constructed. An adaptive algorithm to choose interpolation points at higher computational cost was described in [12]. For the skin effect, prior knowledge of the frequency dependence of the resistance, as well as possible operating frequencies, will allow the selection of the most appropriate frequencies to model the skin effect by the $\sqrt{f}$ formulation.

4. SIMULATION RESULTS

In this section, we present two sets of simulation results to demonstrate the efficiency and accuracy of the proposed method. The first example illustrates delay skew caused by the skin effect in interconnect lines. Consider a 2 GHz clock driving an interconnect line modeled as a distributed RLC circuit. The total capacitance and inductance of the interconnect are 500 fF and 6 nH respectively. The resistance of the interconnect increases from its nearly constant DC value of 240 Ω at 0.1 GHz and reaches 570 Ω at 20 GHz due to the skin effect. The original distributed interconnect model has 100 state variables. The waveform at the far end of the line cannot be computed directly in the time domain since the frequency-dependent resistance couples the time and frequency domains. Hence, we run the FFT with 256 sample points over each clock period to obtain the harmonic frequencies of the input clock. At each harmonic frequency, the frequency-dependent resistance is determined to obtain the interconnect's frequency response over the clock period. With the knowledge of all the harmonic responses, the inverse FFT (IFFT) is run to reconstruct the response of the interconnect in the time domain. This procedure is computationally intensive, especially for large systems.

The reduced interconnect model with 12 state variables was obtained using procedure MPRA and the FFT-based procedure described above was used to obtain the time domain response of the

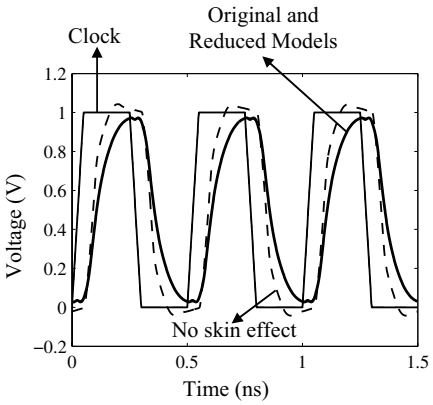

Figure 4: Skin effect in a single interconnect line. Waveforms for the original ($n = 100$, solid curve) and reduced ($n_r = 12$, dotted curve) systems, obtained using a FFT/IFFT procedure, are nearly indistinguishable. Both predict over a 20% delay in comparison to the case when the skin effect is ignored (dashed curve).

reduced system. The interpolation points chosen for the model are $0.1\,\mathrm{GHz}$ and $1\,\mathrm{GHz}$ since the clock frequency is in the GHz range. As shown in Fig. 4, the response of the reduced system matches that of the original system exactly. The overlap of the solid line (which represents the original system) and the dotted line (which represents the reduced system) renders them near indistinguishable from each other. The skin effect causes a 24% increase in delay as measured at $0.5V_{\mathrm{DD}}$ in comparison to the response of the interconnect when the skin effect is ignored (represented by the dashed line in the figure). Further, the figure also illustrates that the voltage response of the interconnect cannot reach the stable voltage points (0 or V_{DD}) in the given clock period. This actually means that the noise margin is reduced when the skin effect in the interconnect is accounted for. Finally, the proposed MOR technique improves simulation speed by 10X for this simple system.

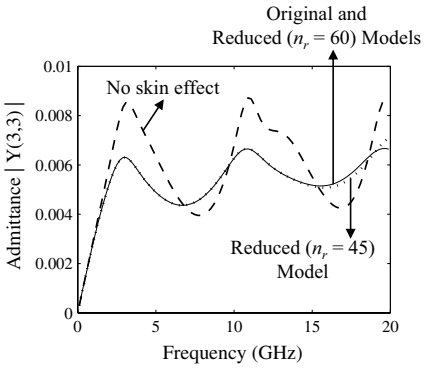

Figure 5: Variation of admittance with frequency of the middle line on a 5-bit wide interconnect bus. The reference (solid curve) is from the original system ($n = 515$). The curve for the reduced model with n_r equals 60 is nearly indistinguishable from that of the original system. For n_r equals 45, there is a small difference between the original system (solid curve) and the reduced system (dotted curve) above $15\,\mathrm{GHz}$. Note also that the admittance in the absence of the skin effect (dashed curve) differs greatly from the original system above $3\,\mathrm{GHz}$.

The second example illustrates a system with 5 high speed interconnect lines that run parallel to each other. The original system, which includes parasitic effects due to coupling capacitance, mutual inductance, and dielectric loss is described using 515 state variables. The resistance increases by a factor of $1.8 \sim 2.4$ from $0.1\,\mathrm{GHz}$ to $20\,\mathrm{GHz}$ when skin effect is considered. The interpolation points chosen to build the reduced system are $0.1\,\mathrm{GHz}$ and $1\,\mathrm{GHz}$. Figure 5 shows the magnitude of one of the components of the 5×5 driving point admittance $\hat{\mathbf{G}}$ matrix of the system. The reduced system of size 60 matches the original system exactly up to $20\,\mathrm{GHz}$ whereas the reduced system of size 45 exhibits a slight divergence after about $15\,\mathrm{GHz}$. Finally, a dashed line is used to plot the admittance when skin effect is ignored. Note that the admittance is essentially the same up to a frequency of about $2.5\,\mathrm{GHz}$ after which there is a divergence of the curves. The verification of the response of this system in both the time and frequency domains through the FFT/IFFT procedure described above is 100X+ faster when the reduced model is used in place of the original model.

5. CONCLUSIONS

In this paper, a rational Arnoldi approach based on multiple interpolation points to handle frequency-dependent effects was presented. The structure $\mathbf{H}(s) = s\mathbf{E} - \mathbf{A} - \mathbf{K}\sqrt{f}$ due to the skin effect in high speed interconnects was preserved in MOR. Our experimental results show that the proposed approach can significantly reduce the complexity of systems with frequency-dependent elements. Simulation of the reduced systems yields highly accurate results at significantly reduced computational cost.

6. REFERENCES

[1] L. T. Pillage and R. A. Rohrer, "Asymptotic waveform evaluation for timing analysis," *IEEE Trans. CAD,* Vol. 9, pp. 352–366, Apr. 1990.

[2] A. Odabasioglu, M. Celik, and L. Pileggi, "PRIMA: Passive reduced-order interconnect macromodeling algorithm," *IEEE Trans. CAD*, Vol. 17, pp. 645–654, Aug. 1998.

[3] P. Feldmann and R. W. Freund, "Efficient linear circuit analysis by Padè approximation via the Lanczos process," *IEEE Trans. CAD,* Vol. 14, pp. 639–649, May 1995.

[4] A. C. Antoulas, "A new result on passivity preserving model reduction," *Systems and Control Letters*, Vol. 54, pp. 361–374, Apr. 2005.

[5] H. Zheng and L. T. Pileggi, "Robust and passive model order reduction for circuits containing susceptance elements," *Proc. ICCAD*, pp. 761–766, 2002.

[6] R. W. Freund, "SPRIM: Structure-preserving reduced-order interconnect macromodeling," *Proc. ICCAD*, pp. 80–87, 2004.

[7] Y. Su, *et al.,* "SAPOR: Second-order Arnoldi method for passive order reduction of RCS circuits," *Proc. ICCAD*, pp. 74–79, 2004.

[8] S. Mei, C. Amin, and Y. Ismail, "Efficient model-order reduction including skin effect," *Proc. DAC*, pp. 232–237, 2003.

[9] R. Achar, M. S. Nakhla, and Q. Zhang, "Full-wave analysis of high-speed interconnects using complex frequency hopping," *IEEE Trans. CAD*, Vol. 17, pp. 997–1016, Oct. 1998.

[10] J. M. Wang, *et al.,* "On projection-based algorithms for model-order reduction of interconnects," *IEEE Trans. Circuits and Systems–I*, Vol. 49, pp. 1563–1585, Nov. 2002.

[11] I. M. Elfadel and D. D. Ling, "A block rational Arnoldi algorithm for multi-point passive model-order reduction of multiport RLC networks," *Proc. ICCAD*, pp. 66–71, 1997.

[12] E. J. Grimme, "Krylov projection methods for model reduction," *Ph.D. thesis,* University of Illinois at Urbana-Champaign, 1997.

[13] R. W. Freund, "Passive reduced-order models for interconnect simulation and their computation via Krylov-subspace algorithms," *Proc. DAC*, pp. 195–200, 1999.